Adaptive secondary mirror demonstrator: design and simulation

J. H. Lee
D. D. Walker
A. P. Doel
University College London
Department of Physics and Astronomy
Optical Science Laboratory
Gower Street
London WC1E 6BT
United Kingdom
E-mail: jhl@star.ucl.ac.uk

Abstract. Atmospheric turbulence distorts the wavefront of the incoming light from an astronomical object and so limits the ability of a telescope to form perfect images. Adaptive optics is a combination of technologies that enable the correction of the wavefront distortion in real time. Conventional adaptive optics operate like auxiliary instruments and use additional relay optics, which reduce total throughput and introduce extra IR emissivity and polarization. Adaptive secondary mirrors avoid additional optical surfaces by providing the optical correction at an existing telescope surface (the secondary mirror). Previous studies have demonstrated the optical efficacy and mechanical feasibility of performing the adaptive correction in this way. A technique demonstrator is being developed to explore features and capabilities applicable to a large adaptive secondary mirror and to explore manufacturing, assembly/disassembly, calibration, and measurement techniques. The paper describes the design of the demonstrator and its predicted performance.
 [S0091-3286(99)00809-0]

Subject terms: adaptive optics; deformable mirror; wavefront corrections; secondary mirror.

Paper 990017 received Jan. 14, 1999; revised manuscript received Mar. 18, 1999; accepted for publication Mar. 25, 1999.

1 Introduction

Adaptive optics systems can be defined as systems that remove the wavefront distortion introduced by the earth's atmosphere by means of one or more optical components introducing a controllable counter wavefront distortion that both spatially and temporally follows that of the atmosphere.[1] Conventional adaptive optics use additional relay optics to form an image of the telescope's pupil, or an image conjugated with one or more nominal turbulent layers in the atmosphere, on one or more deformable mirrors mounted on an optical bench. A separate mirror is also normally included to remove the tip/tilt component of the wavefront distortion separately from the higher-order distortion. Further reimaging optics are then required to bring the light to a focus on the science and wavefront-sensing cameras.

Beckers,[2] in a 1989 telescope proposal to the National Optical Astronomical Observatory (NOAO), proposed using an existing secondary mirror in a telescope as a wavefront correction device for correcting atmospheric distortion. Since the adaptive secondary approach needs no extra relay or reimaging optics, it has several advantages over the conventional approach: (1) optical throughput is greatly enhanced, (2) negligible extra IR emissivity is introduced, which is a crucial advantage for a system intended to operate primarily in the infrared, and (3) no extra polarization is added.

Wavefront tip/tilt correction by the secondary mirror has been implemented at several telescopes. One of the first tip/tilt secondary mirrors was FASTTRAC (Fast Adaptive Secondary for Tip/Tilt Removal by Automatic Centroiding), designed and built by Close and McCarthy.[3] Another tip/tilt secondary mirror has been built for the UKIRT (UK Infra-Red Telescope) 3.8-m telescope in a collaboration between the Royal Observatory Edinburgh (ROE) and the Max-Plank-Institute für Astronomie (MPIA) in Heidelberg.[4] Currently, there is no operating large telescope utilizing a deformable adaptive secondary mirror (ASM). However, a 0.6-m deformable mirror is under development at Steward Observatory and ThermoTrex Corp.[5] Currently two different prototypes of the MMT ASM have been built and tested to investigate system performances.[6]

The Optical Science Laboratory (OSL), through two projects authorized by the UK office of the international Gemini telescope project, have demonstrated the optical efficacy and mechanical feasibility of performing the adaptive correction and IR chopping with an adaptive secondary mirror[7,8] and proposed a design for a 1-m-diam ASM with 90 actuators compatible with possible future requirements of the Gemini project[9] (Fig. 1). This design was shown by finite-element analysis to fit the first 20 Zernike terms and to have acceptable gravity-induced deflections (72 nm) with no additional support system.

Following the previous studies, a technique demonstrator[10] is being developed to evaluate features and capabilities applicable to a large ASM and to explore manufacturing, assembly/disassembly, calibration, and measurement techniques. This report presents the design and predicted performance of the demonstrator.

2 Design

The demonstrator is a 270-mm-diam prototype with seven actuators that is essentially a subsection of the proposed Gemini ASM (Fig. 2) with a sufficient number of degrees of freedom to produce or compensate for several low-order

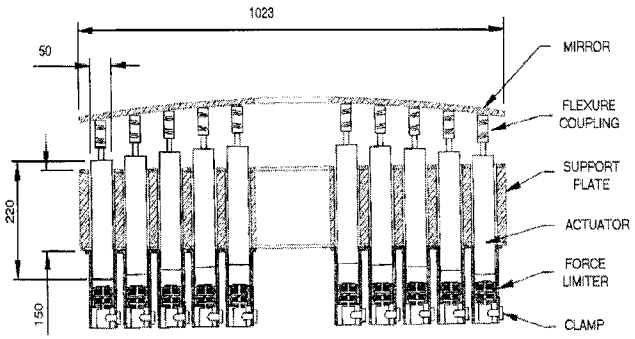

Fig. 1 A design for a possible 1-m-diam ASM with 90 actuators for the Gemini telescope. Dimensions in millimeters.

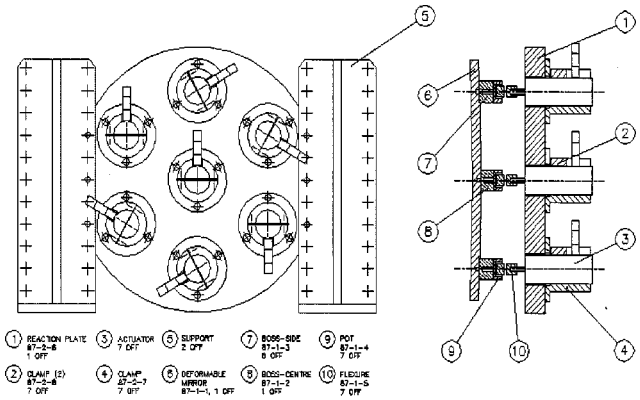

Fig. 3 Mechanical drawing of the assembled demonstrator.

aberrations. The demonstrator has the same actuator spacing (100 mm) and the same mirror substrate and thickness (10-mm-thick aluminum meniscus) as the proposed Gemini design. The diameter of the mirror was chosen as 270 mm to provide minimum gravity deflections on seven actuators and the given actuator spacing.[9]

The principal difference between the proposed Gemini ASM and the demonstrator is that the demonstrator is a concave spherical mirror of radius of curvature of 2.9553 m, rather than a convex mirror. This is (1) for ease of manufacturing and laboratory testing, and (2) so that it may be used directly to relay the Nasmyth focus of the William Herschel Telescope (WHT) in the Ground-based High Resolution Imaging Laboratory (GHRIL).

The design of the demonstrator mirror is shown in Fig. 3. The 10-mm-thick meniscus faceplate has seven tapped blind holes in the back surface to which the actuators are interfaced via flexures. The faceplate, flexures, and reaction plate are all aluminum alloy to minimize thermal distortion. The reaction plate provides the resistance to the reaction forces of the actuators, and the interface to the telescope. It is currently a simple plate for laboratory tests, and it will eventually be replaced with a light-weight stiff aluminum structure. Figure 4 shows a schematic diagram of a flexure coupling between the faceplate and an actuator.

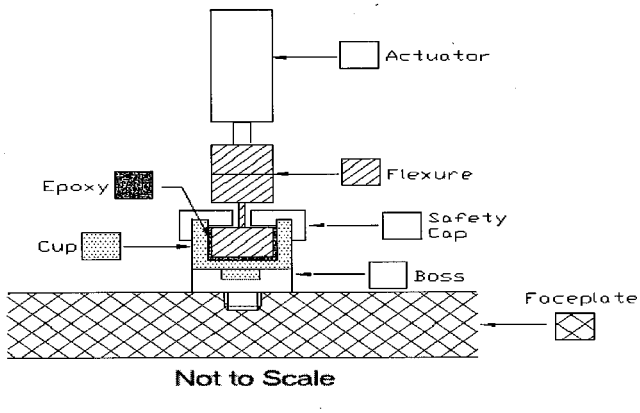

Fig. 4 Schematic diagram of the coupling between the faceplate and an actuator.

3 Finite-Element Analysis

The influence functions of the demonstrator were predicted by finite-element analysis (FEA). Figure 5 shows the FEA-

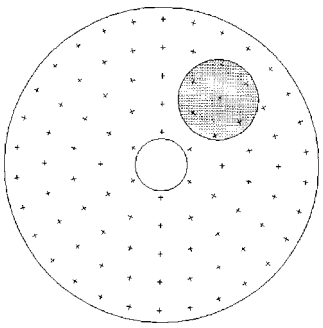

Fig. 2 Drawing of a 1-m mirror, with 90 actuators positioned at the + marks. The small offset circle represents the demonstrator of 270-mm diam with 7 actuators.

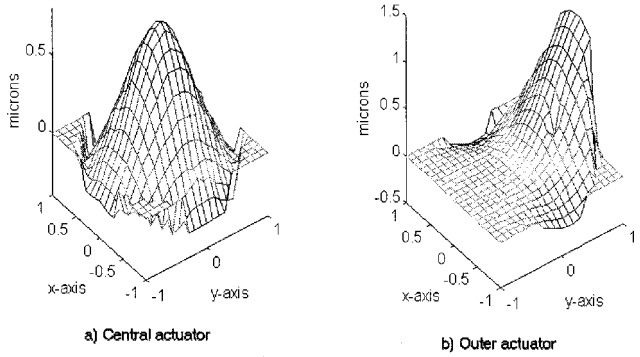

Fig. 5 3-D plots of FEA results: the influence functions.

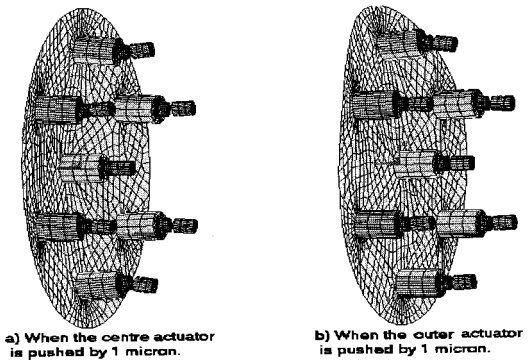

Fig. 6 FEA results on the ASM demonstrator: the deformation of the demonstrator when the central and the outer actuator are pushed by 1 μm.

derived influence functions of the central and outer actuators, each with a stroke of 1 μm.

The deformations of the demonstrator in those cases are shown in Fig. 6. This figure shows the basic idea of how the flexures can provide near-perfect tip/tilt motion, as proven in this paper, while supporting the mirror. Because of the flexures, the demonstrator is able to produce higher-order Zernike modes as well as the lower-order modes without any other supporting structures.

4 Performance Predictions

The performance analysis assumed perfect and instant wavefront sensing and instant wavefront correction, which means the analysis was performed primarily for estimating the fitting errors of the demonstrator.

4.1 *Fitting Error*

An incoming wavefront distortion $\Phi(r,\theta)$ over a circular aperture of arbitrary radius R can be expanded as a linear sum of Zernike polynomials[11] Z_j given by

$$\Phi(R\rho,\theta)=\sum_j a_j Z_j(\rho,\theta), \tag{1}$$

with $\rho=r/R$ and the coefficients a_j being given by

$$a_j=\int \mathrm{d}^2 r\, \rho W(\rho)\Phi(R\rho,\theta)Z_j(\rho,\theta), \tag{2}$$

where the weighting function $W(\rho)$ defining a unit circular aperture is given by

$$W(\rho)=\begin{cases}1/\pi, & \rho\leqslant 1,\\ 0, & \rho>1.\end{cases} \tag{3}$$

If the responses of the actuators are assumed to combine linearly to form the total wavefront correction, the total wavefront correction or the total phase deformation $\Phi_{\mathrm{DM}}(\rho,\theta)$ of the demonstrator can be expressed as a linear sum of the influence functions $F_j(\rho,\theta)$ of the actuators,

$$\Phi_{\mathrm{DM}}(R\rho,\theta)=\sum_j c_j F_j(\rho,\theta), \tag{4}$$

where c_j is the command to the j'th actuator and for a linear control law can be in turn expressed by

$$c_j=\sum_n M_{jn}a_n, \tag{5}$$

where a_n is the coefficient of the n'th Zernike term of the incoming wavefront and M_{jn} are the weightings of the n'th Zernike coefficients. Therefore,

$$\Phi_{\mathrm{DM}}(R\rho,\theta)=\sum_j\left(\sum_n M_{jn}a_n\right)F_j =\sum_n\left(\sum_j M_{jn}F_j\right)a_n=\sum_n a_n\mathcal{Z}_n, \tag{6}$$

where $\mathcal{Z}_n$ is defined as

$$\mathcal{Z}_n=\sum_j M_{jn}F_j. \tag{7}$$

The fitting error E is then given by

$$E(R\rho,\theta)=\Phi(R\rho,\theta)-\Phi_{\mathrm{DM}}(R\rho,\theta) =\sum_j a_j[Z_j(\rho,\theta)-\mathcal{Z}_j(\rho,\theta)]. \tag{8}$$

In turn the mean squared fitting error e^2 over the aperture is given by

$$e^2=\int_0^1 r\,\mathrm{d}r\int_0^{2\pi}\mathrm{d}\theta\, W(r)E(R\rho,\theta)^2. \tag{9}$$

It can also be written in a different form:

$$e^2=\sum_{j=2}^{\infty}a_j^2-\sum_{i=2}^{\infty}\sum_{j=2}^{\infty}a_i a_j(\alpha_{ij}+\alpha_{ji})+\sum_{i=2}^{\infty}\sum_{j=2}^{\infty}a_i a_j\beta_{ij} \tag{10}$$

with

$$\alpha_{ij}=\int_0^1 r\,\mathrm{d}r\int_0^{2\pi}\mathrm{d}\theta\, W(r)Z_i\mathcal{Z}_j, \tag{11}$$

$$\beta_{ij}=\int_0^1 r\,\mathrm{d}r\int_0^{2\pi}\mathrm{d}\theta\, W(r)\mathcal{Z}_i\mathcal{Z}_j. \tag{12}$$

The ensemble-average fitting error is then given by

$$\langle e^2\rangle=\sum_{j=2}^{\infty}\langle a_j^2\rangle-\sum_{i=2}^{\infty}\sum_{j=2}^{\infty}\langle a_i a_j\rangle(\alpha_{ij}+\alpha_{ji}) +\sum_{i=2}^{\infty}\sum_{j=2}^{\infty}\langle a_i a_j\rangle\beta_{ij}. \tag{13}$$

The covariance $C_{ij}=\langle a_i a_j\rangle$ for the atmospheric distortion was derived by Roddier[12] and is shown in Table 1.

Table 1 Covariance matrix C between the first eight Zernike modes, reproduced from Roddier.[12] The units are $(D/r_0)^{5/3}$, where D is the diameter of the entrance pupil of the telescope and r_0 is the coherence length.

0.4557	0	0	0	0	0	−0.0144	0
0	0.4557	0	0	0	−0.0144	0	0
0	0	0.0236	0	0	0	0	0
0	0	0	0.0236	0	0	0	0
0	0	0	0	0.0236	0	0	0
0	−0.0144	0	0	0	0.0063	0	0
−0.0144	0	0	0	0	0	0.0063	0
0	0	0	0	0	0	0	0.0063

4.2 *Choosing the Best-Fit $\mathcal{Z}_j$ of the Demonstrator*

If $\mathcal{Z}_j$ in Eq. (7) is chosen to minimize the mean squared fitting error e^2 [Eq. (9)] for the j'th Zernike term Z_j, then $\mathcal{Z}_j$ can be taken as the best-fit mirror shape for the corresponding j'th Zernike term Z_j. In this case, Eq. (6) gives that the incoming wavefront distortion is decoupled into Zernike terms, and then the command to mirror can be generated in a way to minimize the mean squared fitting error for each Zernike term separately.

One method for constructing mirror shapes for known wavefront distortion is the interaction-matrix approach.[13] An interaction matrix I can be defined so that

$$IA = D, \tag{14}$$

where A is a vector of controlling signals or commands for actuators and D is a vector of wavefront distortion.

The circular aperture of radius R is taken to consist of M small square elements. Then the continuous influence function $F_i(x,y)$ of the i'th actuator can be approximated by a steplike function $\mathcal{F}_i(x,y)$ given by

$$\mathcal{F}_i(x,y) = \sum_{j=1}^{M} a_i^j P(x-x_j) P(y-y_j) \tag{15}$$

with

$$a_i^j = F_i(x_j, y_j), \tag{16}$$

$$P(\Delta x) = \begin{cases} 1 & \text{if} \quad \Delta x \leqslant S/2, \\ 0 & \text{otherwise.} \end{cases} \tag{17}$$

Here S is the width of the square elements (see Fig. 7), and x_j and y_j are rectangular coordinates of the center of the j'th element in the circular aperture. Figure 7 shows an example of the approximation of a circular aperture of radius $R=1$ with 49 elements.

In the same way, the wanted wavefront $\Phi(x,y)$ can be approximated by $\oplus(x,y)$ given by

$$\oplus(x,y) = \sum_{j=1}^{M} b^j P(x-x_j) P(y-y_j) \tag{18}$$

with

$$b^j = \Phi(x_j, y_j). \tag{19}$$

The corresponding vector D of the wavefront distortion is defined by

$$D = (b^1 \quad b^2 \quad \cdots \quad b^M)^T. \tag{20}$$

The interaction matrix I is then given by

$$I = \begin{pmatrix} a_1^1 & a_1^2 & \cdots & a_1^M \\ a_2^1 & a_2^2 & \cdots & a_2^M \\ \vdots & \vdots & \ddots & \vdots \\ a_N^1 & a_N^2 & \cdots & a_N^M \end{pmatrix}. \tag{21}$$

Then the control signal A and the vector $\mathcal{D}$ of the best-fit mirror wavefront are calculated from the pseudoinverse[14] as given by

$$A = \mathcal{I}^{-1} D, \tag{22}$$

$$\mathcal{D} = IA = I\mathcal{I}^{-1} D, \tag{23}$$

where $\mathcal{I}^{-1}$ is the pseudoinverse matrix of the interaction matrix I.

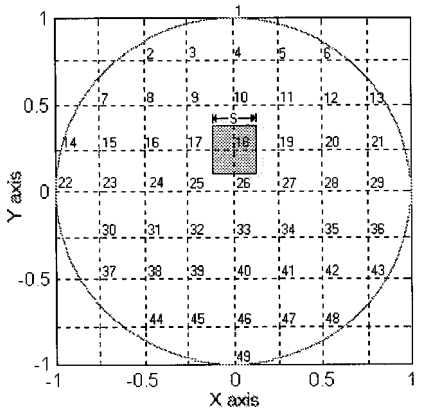

Fig. 7 An example of the approximation of a circular aperture of radius $R=1$ with 49 elements. The shaded region shows the area the 18th element represents. Here S is the width of the square element.

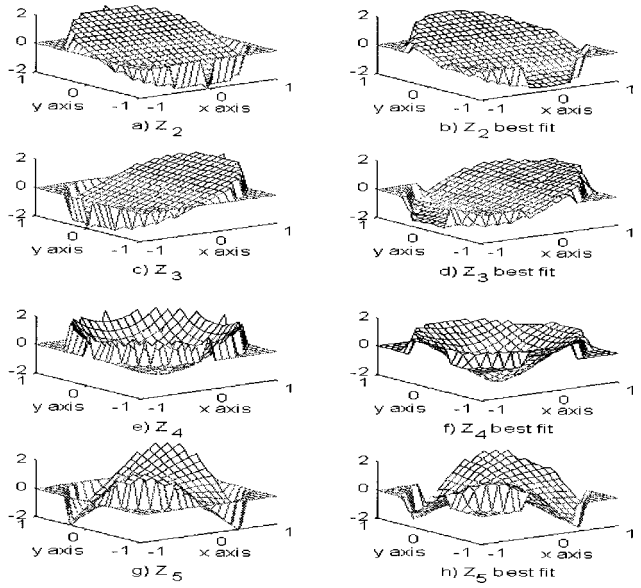

Fig. 8 Zernike terms Z_j (Z_2 through Z_5) and the corresponding best-fit terms $\mathcal{Z}_j$ yielded by the demonstrator.

4.3 *Results*

The first 22 Zernike terms were generated using 50×50 square matrices in a commercial matrix calculation program,[15] and the corresponding best-fit terms $\mathcal{Z}_j$ are derived from Eq. (23) using the FEA-derived influence functions (Fig. 5). The pseudoinverse was calculated using a standard singular-value decomposition (SVD) routine. Several Zernike polynomials Z_j and the corresponding best fits $\mathcal{Z}_j$ are shown in Fig. 8.

Figure 9 shows α_{ij} [Eq. (11)], which represents orthogonality between the i'th Zernike polynomials Z_i and the j'th best fit $\mathcal{Z}_j$. The value of 1 for α_{ij} means a perfect match, while 0 means perfect orthogonality. The graph of β_{ij} [Eq. (12)] is almost identical to that of α_{ij}. The diagonal terms of this plot are redrawn in Fig. 10. This figure shows how well the demonstrator matches the Zernike polynomials. Figure 10 shows that tip/tilt modes are almost perfectly fitted, and defocus up to a 90% level. The results also show excellent correction for astigmatism. Interestingly, the 10th Zernike term (trefoil) is 90% corrected, but the 9th Zernike term, which represents the other orthogonal component of trefoil, is not corrected at all. In one case the six actuators in the circle coincide with the three peaks and three valleys in the wavefront. In the other they coincide with the zero points between the peaks and valleys and therefore have no effect. The demonstrator is also shown not to have enough degrees of freedom to compensate coma (the 7th and 8th Zernike terms).

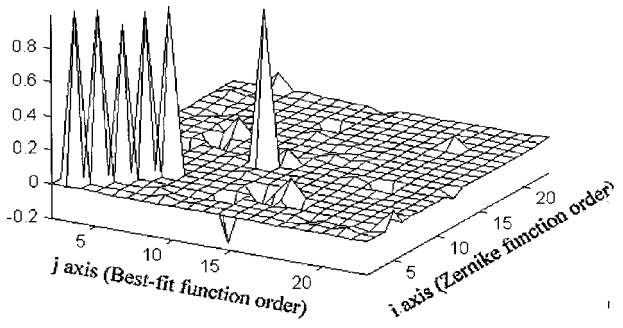

Fig. 9 Elements α_{ij} [Eq. (11)] between the first 22 Zernike terms Z_j and the best-fit terms $\mathcal{Z}_j$. This figure represents orthogonality between the i'th Zernike terms Z_i and the j'th best-fit terms $\mathcal{Z}_j$. In this plot, a z-axis value of 1 means perfect matching, while 0 means perfect orthogonality.

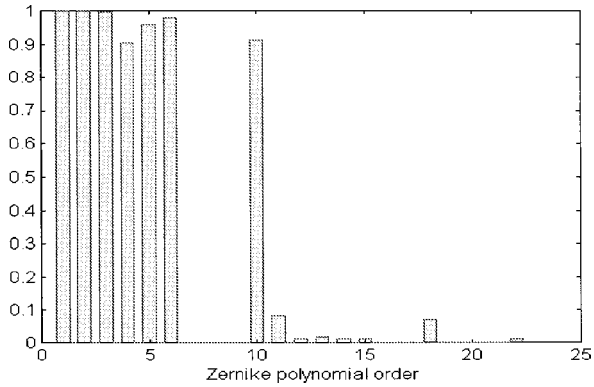

Fig. 10 Diagonal elements α_{jj} [Eq. (11) and Fig. 9] between the first 22 Zernike terms Z_j and the best fits $\mathcal{Z}_j$. This plot shows how well the mirror matches the Zernike polynomials. A z-axis value of 1 means perfect matching, while 0 means zero ability to fit the term.

Using the previous results and Eq. (13), the resultant ensemble-average fitting error for the first 22 Zernike terms is calculated as

$$\langle e^2\rangle = 0.021\left(\frac{D}{r_0}\right)^{5/3} \quad \text{rad}^2, \tag{24}$$

and the total resultant residual error, including the Zernike-Kolmogoroff residual errors,[11] is

$$\langle e^2\rangle = 0.042\left(\frac{D}{r_0}\right)^{5/3} \quad \text{rad}^2. \tag{25}$$

The corresponding Strehl ratio[16] is approximately given by

$$\text{Strehl ratio} = \exp(-\langle e^2\rangle) = \exp\left[-0.042\left(\frac{D}{r_0}\right)^{5/3}\right]. \tag{26}$$

Figure 11 plots the Strehl ratio against the various D/r_0, where D is the diameter of the entrance pupil and r_0 is the coherence length.

5 Conclusion

The design of the demonstrator is unique in that it does not have extra supporting structures for the mirror, and the flexure coupling is a key factor that makes this possible. The design including the flexure-coupling component was proven by FEA to provide near-perfect tip/tilt motion. Since the tip/tilt modes are responsible for 87% of the incoming atmospheric distortion and the tip/tilt motion of the demonstrator is not a simple rigid-body motion due to the

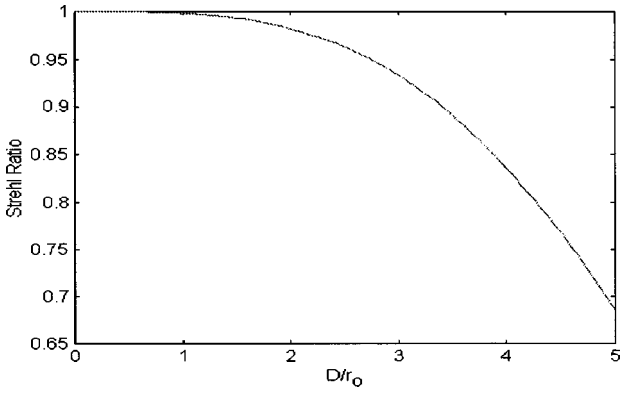

Fig. 11 Strehl ratio of the demonstrator.

mechanical moment by the flexures, the importance of the fact that the demonstrator can reproduce near perfect tip/tilt cannot be overemphasized.

The demonstrator was also shown to have an ensemble residual fitting error for atmospheric correction given by

$$\langle e^2 \rangle = 0.042 \left(\frac{D}{r_0} \right)^{5/3} \quad \text{rad}^2 \tag{27}$$

so the demonstrator can achieve the Strehl ratio of 0.43 for IR imaging (2.2 μm) at the 4.2-m WHT under five-percentile seeing ($r_0 = 0.7$ m at 2.2 μm).[17]

For a very large telescope of diameter of $\approx$8 m, it is no longer simple to scale the performance of the demonstrator directly to a real adaptive secondary, since proportionally more energy is propagated on higher-order Zernike terms due to the finite outer scale of the atmospheric turbulence. Therefore, the exact performance of the ASM for a very large telescope should be studied further in future. However, Eq. (27) still provides a baseline performance even for a very large ASM.

In conclusion, this work has successfully confirmed the viability of the design, including the flexure-coupling component, and given a baseline prediction of the wavefront correction performance of the demonstrator.

Acknowledgments

The work described in this paper has been financed from a number of sources, including the Satellite Technology Research Center (SaTReC) of the Korea Advanced Institute of Science and Technology (KAIST), the UK Gemini project office, and the UK Particle Physics and Astronomy Research Council.

References

1. J. M. Beckers, ''Adaptive optics for astronomy: principles, performance and applications,'' *Annu. Rev. Astron. Astrophys.* **31**, 13–62 (1993).
2. J. M. Beckers, ''A proposal to the National Science Foundation,'' in *The NOAO 8-M Telescope Technical Description, Vol. II*, Association for University Research in Astronomy (1989).
3. L. M. Close and D. W. McCarthy, ''High-resolution imaging with a tip/tilt Cassegrain secondary,'' *Publ. Astron. Soc. Pac.* **106**, 77–86 (Jan. 1994).
4. E. Pitz, R. R. Rohloff, and H. Marth, ''UKIRT 5-axis tip/tilt secondary electro-mechanical and optical design,'' in *Proc. ESO*, Garching, Germany (1993).
5. D. G. Bruns, T. K. Barrett, and D. G. Sandler, ''MMT adaptive secondary mirror prototype performance,'' *Proc. SPIE* **2871**, 890–896 (1996).
6. P. Salinari and D. G. Sandler, ''High order adaptive secondary mirrors: Where are we?,'' *Proc. SPIE* **3353**, 742–753 (1998).
7. D. D. Walker, R. G. Bingham, and B. C. Bigelow, ''Adaptive correction at telescope secondary mirrors,'' in *Proc. ESO*, No. 48, pp. 255–260 (1993).
8. B. C. Bigelow, D. D. Walker, R. G. Bingham, and P. D'Arrigo, ''A deformable secondary mirror for adaptive optics,'' in *Proc. ESO*, No. 48, pp. 261–266 (1993).
9. B. C. Bigelow, D. D. Walker, and R. G. Bingham, ''Design of an adaptive secondary mirror, phase II: Zernike polynomial fitting to mirror FEA models and design of a 270 mm demonstrator mirror,'' Report to the Gemini-UK Project at Oxford (Apr. 1994).
10. D. D. Walker, J. H. Lee, R. G. Bingham, D. Brooks, M. Dryburgh, G. Nixon, H. Jamshidi, S. W. Kim, and B. Bigelow, ''Rugged adaptive telescope secondaries: experience with a demonstrator mirror,'' *Proc. SPIE* **3353**, 872–878 (1998).
11. R. J. Noll, ''Zernike polynomials and atmospheric turbulence,'' *J. Opt. Soc. Am.* **66**(3), 207–211 (1976).
12. N. Roddier, ''Atmospheric wavefront simulation and Zernike polynomials,'' *Proc. SPIE* **1237**, 668–679 (1990).
13. R. K. Tyson, *Principles of Adaptive Optics*, Academic Press, San Diego, CA (1991).
14. D. J. Scott, *A Course in Linear Algebra with Applications*, World Scientific, Singapore (1991).
15. MATLAB, The MathWorks, Inc., 24 Prime Park Way, Natick, MA.
16. W. J. Smith, *Modern Optical Engineering*, 2nd ed., pp. 151–155, McGraw-Hill (1990).
17. S. W. Unger, *PPARC-NWO Joint Steering Committee Director*, http://ing.iac.es/director/jsc9703.html

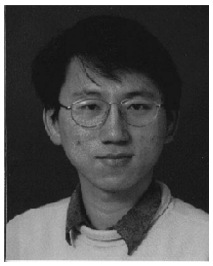

J. H. Lee received his BSc degree from the Mechanical Engineering Department of the Korea Advanced Institute of Science and Technology (KAIST) in 1994, and his MSc degree with distinction in satellite communication and spacecraft technologies from University College London (UCL) in 1995. He then received the PhD in adaptive optics from UCL in 1999. During his PhD work, he was also involved in the development of a spaceborne camera.

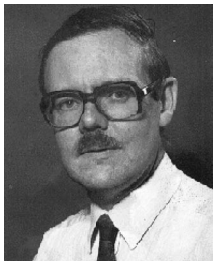

D. D. Walker received his PhD in astronomical instrumentation for ground-based telescopes from UCL in 1980. He subsequently developed cryogenic CCD cameras, and then led the development of the UCL Echelle Spectrograph for the Anglo Australian Telescope. In 1985 he became the founding director of the Optical Science Laboratory at UCL, a post he continues to fill. He has led numerous other instrumentation projects and is currently the Principal Scientist for the Gemini High Resolution Optical Spectrograph. His research interests are focused on systems-level optimization of instrumentation, applied over a broad range of applications, in particular adaptive optics, optical production, and metrology. He is also a founding director of a spin-off company Optical Generics Ltd, which is producing commercial machines for grinding and polishing aspheric optics.

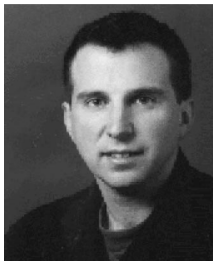

A. P. Doel received his PhD in adaptive optics for large ground-based telescopes from the University of Durham in 1990. He then joined the Astronomical Instrumentation Group in Durham as a post-doctoral research assistant, where he worked on the MARTINI, ELECTRA, and NAOMI adaptive optics systems for the 4.2-m William Herschel Telescope on La Palma, Canaries. In 1998 he took up a lectureship at the Optical Science Laboratory at UCL, where he heads the adaptive optics division. His research interests include atmospheric turbulence modeling and adaptive optics for astronomical and industrial uses.